RSC Advances

PAPER

View Article Online
View Journal | View Issue

Cite this: *RSC Adv.*, 2021, **11**, 24762

Promoted activity of annealed Rh nanoclusters on thin films of Al_2O_3/NiAl(100) in the dehydrogenation of Methanol-d_4†

Ting-Chieh Hung,[a] Ting-Wei Liao,[a] Guan-Jr Liao,[a] Zhen-He Liao,[a] Po-Wei Hsu,[a] Yu-Ling Lai,[b] Yao-Jane Hsu,[b] Chia-Hsin Wang,[b] Yaw-Wen Yang,[b] Jeng-Han Wang[c] and Meng-Fan Luo*[a]

Annealed Rh nanoclusters on an ordered thin film of Al_2O_3/NiAl(100) were shown to exhibit a promoted reactivity toward the decomposition of methanol-d_4, under both ultrahigh vacuum and near-ambient-pressure conditions. The Rh clusters were grown with vapor deposition onto the Al_2O_3/NiAl(100) surface at 300 K and annealed to 700 K. The decomposition of methanol-d_4 proceeded only through dehydrogenation, with CO and deuterium as products, on Rh clusters both as prepared and annealed. Nevertheless, the catalytic reactivity of the annealed clusters, measured with the production of either CO or deuterium per surface Rh site from the reaction, became at least 2–3 times that of the as-prepared ones. The promoted reactivity results from an altered support effect associated with an annealing-induced mass transport at the surface. Our results demonstrate a possibility to practically prepare reactive Rh clusters, regardless of the cluster size, that can tolerate an elevated reaction temperature, with no decreased reactivity.

Received 25th May 2021
Accepted 12th July 2021

DOI: 10.1039/d1ra04066a

rsc.li/rsc-advances

Introduction

The catalytic decomposition of methanol (CH_3OH) is extensively investigated because the principal reaction can serve as a source of hydrogen and also be applied in direct methanol fuel cells (DMFCs), which offer a prospect of efficient conversion of methanol to electricity.[1–9] As the production of hydrogen or the performance of DMFCs is governed largely by the catalytic reaction, promoting the reactivity of catalysts becomes desirable. Varied strategies have been attempted, such as creating defects and active atoms on the topmost surfaces to increase the reaction centers,[10–12] or fine-tuning the electronic state of metal clusters by alloying another metal.[13] Annealing is a common approach to modify catalysts structurally and thus their reactivity. Preceding works showed that annealing can alter the morphology, size and structures of oxide-supported nanoclusters;[14–29] annealing can also induce mass transport and thus encapsulation and oxidation of oxide-supported nanoclusters.[23,30–38] On the other hand, the thermal stability of catalysts, reflected in the annealing-induced variation of structures and reactivity, is a major concern for qualified catalysts.[14–18] The objective of the present work was to study the effect of annealing on the reactivity of oxide-supported rhodium (Rh) clusters in the decomposition of methanol. Rh catalysts have been widely used and studied,[39–42] whereas realistic model systems, Rh nanoclusters supported on structurally well-defined oxides,[43,44] for methanol reactions and the annealing effect have been little investigated. The present work has an aim to remedy this lack and to acquire insights into the effect.

We investigated the decomposition of methanol-d_4 (CD_3OD) on Rh clusters supported on an ordered thin film of Al_2O_3/NiAl(100), under both ultrahigh vacuum (UHV) and near-ambient-pressure conditions, and with various techniques to probe the surface. The Rh clusters were prepared by depositing a vapor onto Al_2O_3/NiAl(100) at 300 K and annealing to 700 K. The thin film Al_2O_3/NiAl(100) was used as a support in our model system because it resembles various physical properties that are characteristic of the bulk Al_2O_3 (a popular catalyst support) and allows the use of electron-based surface probe techniques.[44–52] Methanol-d_4, rather than methanol (CH_3OH), was used because this isotopic variant has similar properties, such as adsorption energies and activation energies for decomposition (determined by their electronic structures), but the former gave clearer signals of molecular deuterium (D_2), an essential product to reveal the reaction mechanisms, in temperature-programmed desorption (TPD) experiments. The morphology and structure of the Rh clusters were characterized

[a]*Department of Physics, National Central University, 300 Jhongda Road, Jhongli District, Taoyuan, 32001, Taiwan. E-mail: mfl28@phy.ncu.edu.tw*

[b]*National Synchrotron Radiation Research Center, 101 Hsin-Ann Road, Hsinchu Science Park, Hsinchu 30076, Taiwan*

[c]*Department of Chemistry, National Taiwan Normal University, No. 88, Sec. 4, Ting-Zhou Road, Taipei, 11677, Taiwan*

† Electronic supplementary information (ESI) available: Additional TPD and IRAS data. See DOI: 10.1039/d1ra04066a

with scanning tunnelling microscopy (STM), reflection high-energy electron diffraction (RHEED) and synchrotron-based photoelectron spectroscopy (PES); the catalyzed reactions were monitored with infrared reflection absorption spectroscopy (IRAS), TPD, synchrotron-based near ambient pressure X-ray photoelectron spectroscopy (APXPS).

The characterization shows that methanol-d_4 on the Rh clusters, with a mean diameter 1.0–3.5 nm and height 0.6–0.8 nm, decomposed through only one channel – dehydrogenation to CO, whereas the production of CO and D_2 per surface Rh site from the reaction, corresponding to the reactivity, was significantly promoted on the annealed Rh clusters. This promotion was generally observed for clusters of diameter >1.2 nm, not only under UHV conditions but also near ambient pressure. An analogous reactivity promoted on annealing was observed on supported neither Pt nor Pd clusters,[23,34,47,53–55] For a comparable system Pt clusters on Al_2O_3/NiAl(100), annealing induced oxidation and alumina encapsulation of the Pt clusters but no promotion in reactivity; instead, the dehydrogenation was hindered to a certain extent.[23,34] We argue that the annealing on the present system caused considerable mass transport, the diffusion of Rh to the substrate and the migration of alumina to the clusters, and thus created new oxide–Rh interfaces providing additional active sites. As annealing constantly causes sintering and encapsulation of oxide-supported clusters, which increases cluster sizes, decreases active surface sites and alters surface electronic states, it typically decreases the reactivity of the clusters.[17,18,37,38,56] The present results demonstrate a contrasting case, in which an altered metal–support interaction promotes the reactivity, and also imply a practical method to engineer reactive Rh clusters, which does not decay in reactivity even when the reaction proceeds at elevated temperature.

Experimental methods

Our experiments were primarily performed in UHV chambers with a base pressure in a 10^{-10} torr regime. A NiAl(100) sample (MaTeck GmbH) was polished to a roughness less than 30 nm and an orientation accuracy better than 0.1°; a Rh(100) sample (MaTeck GmbH) was polished to an orientation accuracy better than 1°. To obtain a clean surface, the sample underwent alternative cycles of sputtering and subsequent annealing before each experiment. The cleanliness of the sample was monitored with Auger electron spectroscopy, low-energy electron diffraction and STM. An ultra-thin θ-Al_2O_3 film was formed on oxidation of a NiAl(100) alloy surface at 1000 K; the formation of Al_2O_3 thin films is described elsewhere.[45,46,48,49] To achieve a homogeneous crystalline Al_2O_3 surface with no NiAl facets,[57,58] we refrained from protracted post-oxidation annealing of the oxide films. The amorphous oxide surface was also negligible. The grown θ-Al_2O_3 thin film had thickness 0.5–1.0 nm.[45,49] The sample was then quenched to 300 K for vapor deposition of Rh from an ultra-pure Rh rod (Goodfellow Cambridge Ltd, 99.9%) heated by electron bombardment in a commercial evaporator (Omicron EFM 3). The rate of deposition of Rh was fixed about 0.15 ML min^{-1}, calculated according to the coverage prepared at 300 K. The coverage was estimated from the volume of the Rh clusters observed with STM; 1.0 ML corresponds to a density 1.39×10^{15} atoms per cm^2 of fcc Rh(100) surface atoms. After the deposition, the sample was cooled to the desired adsorption temperature (100 K, unless specified). Methanol and CO gases were dosed by a doser pointing to the sample, with a background pressure 2–5 $\times 10^{-9}$ torr. The highly pure methanol and methanol-d_4 (Merck, 99.8%) were additionally purified by repeated freeze–pump–thaw cycles before being introduced into the UHV chambers. We report methanol and CO exposures in Langmuir units (1 L = 10^{-6} torr s).

STM images (recorded with a RHK UHV 300 unit), constant-current topographies, were obtained at 90 K with a sample bias voltage typically 2.4–2.8 V and a tunneling current 0.8–1.2 nA. The STM tip consisted of an electrochemically etched tungsten wire. RHEED was performed with an incident electron beam of energy 40 keV at a grazing angle 2°–3° to the surface. TPD spectra were taken by ramping up the sample temperature at 3 K s^{-1} and monitoring the various masses on a quadrupole mass spectrometer (Hiden), which was shielded and placed close (about 2 mm) to the sample. IRAS spectra were collected using a Fourier transform infrared spectrometer (FTLA 2000) with external optics aligned for an incident angle 75° from the sample normal, and a liquid nitrogen-cooled MCT detector. The IRAS spectra are presented as the ratio of sample and oxide surface (or Rh clusters) data measured at the same surface temperature (100 K), and are typically the average of 256 scans at resolution 4 cm^{-1}. The PES and APXPS experiments were performed at the TLS BL09A2 and 24A beamlines, respectively, at National Synchrotron Radiation Research Center in Taiwan.[59,60] For the former, the beam (a fixed energy 383 eV) was incident normal to the surface and photoelectrons were collected at angle 58° from the surface normal; for the latter, the beam (a fixed energy 380 eV) was incident 56° from the surface normal and the analyzer (SPECS NAP 150), coupled with 4-stages differential pumping, was placed normal to the surface. The energy resolution was estimated to be near 0.1 eV and the binding energy (BE) is referred to the substrate bulk Al 2p core-level at 72.9 eV.[61–63] All photoelectron spectra presented here were normalized to the incident photon flux. The gaseous reaction products during the APXPS experiments were concomitantly measured by a quadrupole mass spectrometer (Hiden), accommodated in a doubly-differentially pumped chamber with a stainless steel tubing inlet terminated with an aperture (300 μm dia. at 1 cm from the sample). The data were presented with averages values of 300 s.

Results

Morphology and structure of supported Rh clusters

The Rh clusters were grown from deposition of a vapor on Al_2O_3/NiAl(100) at 300 K and annealed to 700 K; they were characterized structurally with STM and RHEED. The annealing temperature 700 K was employed as the sample annealed to such temperature exhibited limited sintering but evident promotion of reactivity; a lower annealing temperature, such as

450 and 570 K, failed to promote the reactivity equally whereas a higher one, such as 800 K, induced evident sintering.[64] The Rh clusters as prepared had a mean diameter from 1.0 to 3.5 nm and a height from 0.4 to 0.8 nm evolving with the coverage;[44] with the annealing to 700 K, the morphology of neither large nor small clusters altered a lot but the cluster density decreased significantly. Our previous work had demonstrated the structural and morphological evolution of the Rh clusters with the annealing (450–800 K).[64] Fig. 1a and b exemplify the annealing-induced alteration of Rh clusters on Al_2O_3/NiAl(100). The insets in the figures show characteristic histograms of the height and diameter for each temperature; the curve in each histogram is a Gaussian fit to the size distribution. At 300 K, Rh clusters (1.6 ML) had a mean diameter about 2.3 nm and height about 0.8 nm (Fig. 1a); with the temperature increased to 700 K, both the mean diameter and height altered little but the cluster density decreased notably – the total surface Rh decreased by about 30%. The observation implies that the cluster dissociation was active at 700 K and a significant proportion of Rh atoms from the dissociated clusters diffused into the substrate, likely through surface defects.[1,47,53,54] The Rh diffusion into the substrate also prevents the growth of the clusters and the nucleation into new clusters, so the typical sintering feature, a bimodal size distribution, was not evident at this temperature. The comparison of diameters of the clusters as prepared and annealed (0.5–4.0 ML) is shown in Table S1 (ESI†).

The clusters as prepared were structurally ordered and became even more ordered – the content of the ordered structures increased – after the annealing, indicated by their RHEED patterns. Fig. 2 exemplifies the patterns and the annealing effect on the structures. The reflection rods in the RHEED patterns (Fig. 2a) are ascribed to the oxide and to the NiAl(100) substrate; the half-order reflections indicate the (2×1) structure of the ordered θ-Al_2O_3(100).[45,46,48,49] The patterns superimposed on the reflection rods at azimuths [0−10] and [0−11] resulted from structurally ordered Rh clusters (Fig. 2a and b). They had an fcc phase and grew with their facets (100) parallel to the θ-Al_2O_3(100) surface; their [110] axes lay along direction [010] of the oxide surface, so Rh(100)[110]//Al_2O_3(100)[010]. This orientation is preferred because the (100) facets of the Rh clusters match structurally better the square oxygen lattice of the θ-Al_2O_3(100) surface.[23,58,65] The lattice parameter of the Rh clusters also increased to match the oxide surface; relative to bulk Rh, it increased up to 6% with decreasing cluster size. After elevating temperature to 700 K, the pattern became sharper (Fig. 2c and d), indicating an increased content of the ordered structures; the cluster orientation remained but the lattice parameter decreased by about 1.5% (from 3.92 to 3.86 Å). The decreased lattice parameter was typically ascribed to an attenuating substrate effect resulting from increased cluster sizes, whereas in the present case the clusters were not enlarged. The decreased Rh–Rh distance (toward their bulk value) could result from an altered metal–support interaction, described below. The similar decrease of the lattice parameter was also observed for Rh clusters at other coverages (Table S1†).

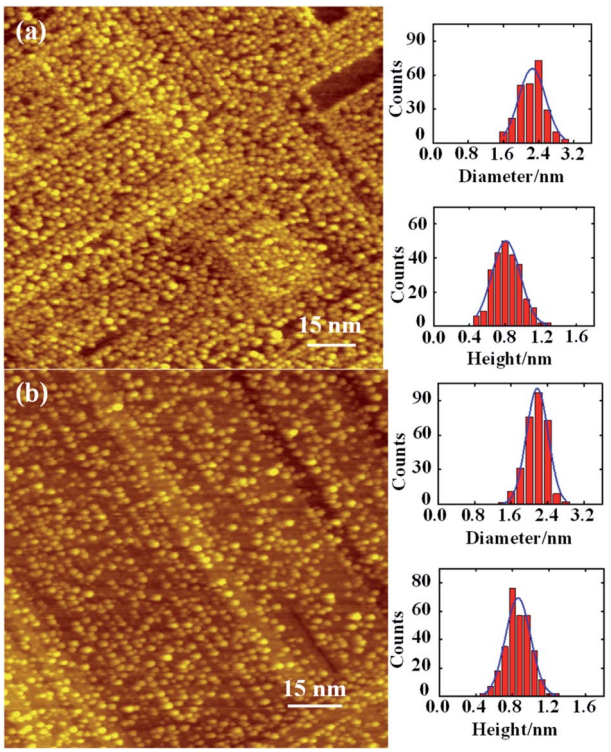

Fig. 1 STM images for 1.6 ML Rh deposited on a thin film of Al_2O_3/NiAl(100) at (a) 300 K and annealed to (b) 700 K. The insets in (a) and (b) show characteristic histograms of height and diameter for each temperature; the curves are the best Gaussian fits to the distributions.

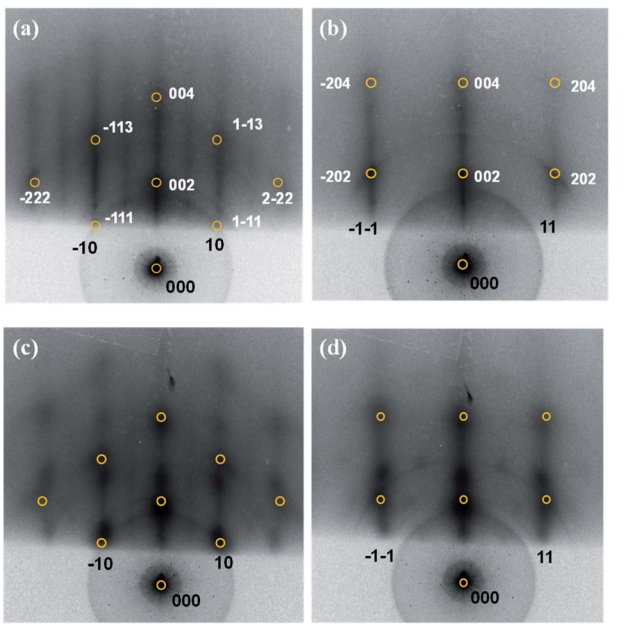

Fig. 2 RHEED patterns for 4.0 ML Rh deposited on Al_2O_3/NiAl(100) at (a and b) 300 K and annealed to (c and d) 700 K. (a and c) Show patterns obtained at azimuth [0−10] of NiAl substrate, and (b and d) at azimuth [0−11]. Yellow circles denote reciprocal-lattice points for the clusters of Rh(001)[110]//Al_2O_3(100)[010].

We noted that additional diffraction spots emerged with the elevated temperature, along the reflection rods of NiAl or alumina oxides, such as (10) and (11), for high Rh coverages (≥3.0 ML), as shown in Fig. 2c and d. These patterns are modulated reflection rods from NiAl or alumina films, largely due to a roughening oxide surface.[23,34] This roughening arose from considerable mass transport, including not only diffusion of Rh atoms into the substrate (indicated in the above STM images) but also migration of alumina materials (Al_xO_y) to the Rh clusters, as observed for Pt clusters on Al_2O_3/NiAl(100).[23] The mass transport could alter the interaction between Rh and alumina, as indicated in Pt clusters on Al_2O_3/NiAl(100),[23] and produce new Rh–alumina interfaces, despite the interior of Rh clusters remained in an fcc structure and became structurally more ordered. The modulated reflection rods appeared only at greater Rh coverages, because of limited sensitivity of RHEED; the mass transport was expected to occur for smaller Rh coverages as well. Annealing to a lower temperature, such as 450 and 570 K, yielded no comparably modulated reflection rods; the mass transport was apparently a thermally activated process.

Decomposition of methanol or Methanol-d_4 on supported Rh clusters

The reaction of methanol-d_4 on the supported Rh clusters was characterized primarily with TPD, APXPS and IRAS. As the decomposition of methanol-d_4 on supported Rh clusters proceeded only through dehydrogenation,[44] we monitored the reactivity with the desorption spectra of CO and D_2. The alternative channel, scission of the C–O bond in methanol-d_4, remained closed on the annealed Rh clusters as no CD_4 signal was observed. Moreover, the dehydrogenation must have occurred on the supported Rh clusters, as desorption of neither CO nor D_2 was observed for methanol-d_4 on Al_2O_3/NiAl(100).[55]

Fig. 3a and b parallel the CO TPD spectra from molecularly adsorbed CO (grey) and produced CO (denoted as CO_m) from dehydrogenated methanol-d_4 (black) on Rh clusters (1.0 and 4.0 ML) as prepared and annealed on Al_2O_3/NiAl(100). The molecularly adsorbed CO was prepared on exposing the sample to 2.0 L CO at 100 K, which sufficed to saturate the surfaces of the clusters; the CO_m was from the sample exposed to 2.0 L CD_3OD, for which a multilayer of methanol-d_4 formed on the surface. The signals between 100 and 200 K arose from either the background or the cracking patterns of desorbing methanol-d_4.[44,55] The CO desorption ranged from 300 to 550 K, resembling that from Rh single crystals and clusters.[39–41,66,67] No CO (or CO_m) desorbed from the Al_2O_3/NiAl(100) surface, as the adsorption temperature for CO on Al_2O_3/NiAl(100) is below 100 K.[68] As adsorbed methanol-d_4 decomposed to CO_m far below 300 K (indicated by the IRAS spectra below), CO_m moved to preferred sites and desorbed as molecularly adsorbed CO. For 1.0 ML Rh clusters (mean diameter 1.7 nm) as prepared (Fig. 3a lower), the integrated intensity of desorption of CO_m (black) was about half that of molecularly adsorbed CO (grey); the fraction increased to about 75% (upper in Fig. 3a) on the clusters annealed to 700 K. A similar enhancement was observed for clusters of other sizes. Fig. 3b shows that on larger clusters (4.0 ML, mean diameter 3.5 nm), the fraction was enhanced from about 40% to above 90%. As the desorption intensity of molecularly adsorbed CO serves as a rough measure of the number of surface Rh sites, the result indicates that the production of CO_m per surface site, corresponding to the reactivity, was enhanced on the annealed Rh clusters.

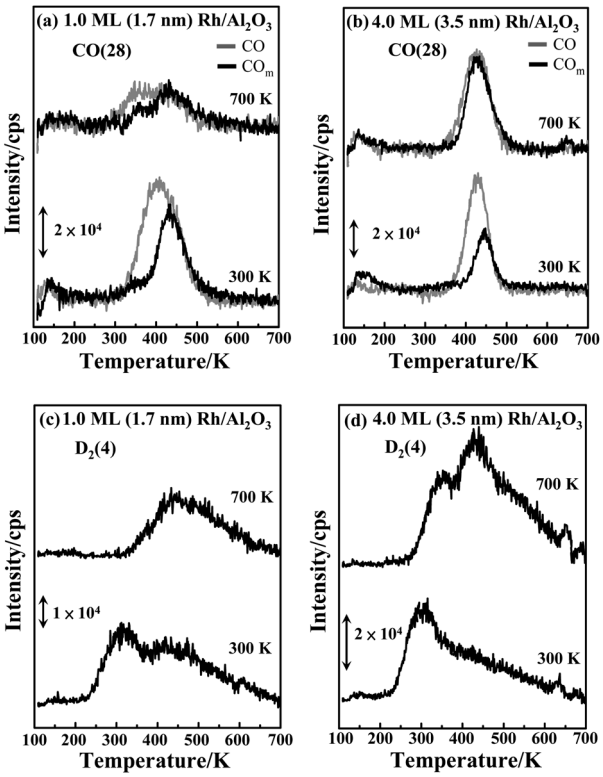

Fig. 3 TPD spectra of (a) and (b) CO ($m/z = 28$ u) and (c) and (d) D_2 ($m/z = 4$ u) from 2.0 L CD_3OD adsorbed on 1.0 and 4.0 ML Rh clusters/Al_2O_3/NiAl(100) as prepared at 300 K (lower panels) and annealed to 700 K (upper panels). The grey lines in (a) and (b) indicate the CO TPD spectra from 2.0 L CO molecularly adsorbed on the 1.0 and 4.0 ML Rh clusters at 100 K. The 1.0 and 4.0 ML Rh clusters had mean diameters 1.7 and 3.5 nm respectively, indicated in the figure.

The D_2 signals from dehydrogenated methanol-d_4 show a consistent picture. On Rh clusters as prepared, D_2 desorbed between 250 and 700 K (bottom, Fig. 3c and d): a maximum about 300 K and a shoulder about 450 K and extending to 700 K. On the annealed clusters, the D_2 signal about 300 K almost vanished whereas that about 450 K either remained (1.0 ML) or increased (4.0 ML) (upper panels, Fig. 3c and d). The D_2 desorption shifted in general to higher temperature (ESI, Fig. S1†). The line shape changed considerably because the interaction of D atoms with the surfaces altered; new surface sites, having a stronger bonding with D atoms, were created by the annealing. The new sites are likely Rh–O intermixing ones at the Rh–oxide interface and have bonding-unsaturated O and Rh, which form a stronger bond with D atoms. The integrated intensities of the D_2 lines showed that the D_2 produced per surface site also increased. For 4.0 ML clusters, as the number of surface sites of the Rh clusters altered little (grey lines in

Fig. 3b), the evidently increased D_2 signal indicates an increased production of D_2 per surface site. Annealed 1.0 ML clusters gave no increased D_2 signals, but their ratio of D_2 to CO signals increased since the surface sites of the annealed Rh clusters decreased, indicating also an enhanced reactivity.

Fig. 4a plots the ratio of the desorption intensities of CO_m and molecularly adsorbed CO on the clusters as prepared (300 K) and annealed (700 K), for varied initial Rh coverages. The Rh coverages 0.5–4.0 ML correspond to the clusters of diameters 1.4–3.5 nm, indicated in the figure. The ratios for 0.13 and 0.25 ML Rh (diameter $\leq$ 1.2 nm) are near 1.0 at 300 K (dashed line in Fig. 4a); after the annealing to 700 K, the remaining Rh clusters were too few to give reliable signals. For larger Rh clusters, the annealing improved the reactivity significantly; the ratios for these annealed clusters were increased to above 0.75 (about 0.4 for as-prepared ones). Similar improvement was also reflected on the ratios of the desorption intensities of D_2 and molecularly adsorbed CO (Fig. 4b). Both the ratios CO_m/CO and D_2/CO for the annealed clusters became 2–3 times those for the as-prepared ones. As the ratios correspond to the production of CO_m and D_2 per surface Rh site, the increased ratios reflect a promoted reactivity toward methanol-d_4 decomposition. Additionally, except the small clusters (diameters $\leq$ 1.2 nm, coverages $\leq$ 0.25 ML), the promotion depended little on the cluster size. To corroborate the results, we estimated also the number of surface sites with the surface area of the Rh clusters measured with STM. The estimate, which complements the above TPD approach,[68,69] shows a consistent trend: the production of either CO_m or D_2 per surface site increased on the annealed clusters, 2–6 times (Fig. S2†). Moreover, the ratio of CO_m/D_2 from the clusters as prepared and annealed remained nearly constant, indicating no additional reaction channel involved in the promoted reactivity.

Fig. 5 compares CD_3OD TPD spectra from 2.0 L CD_3OD adsorbed on a Rh(100) surface, 4.0 ML Rh clusters/Al_2O_3/NiAl(100) as prepared and annealed. A distinct feature between 110 and 150 K in the spectra is attributed to desorption of multilayer methanol-d_4 as the feature was never saturated and was observed on varied surfaces.[50,55,70–72] A separate maximum centered about 160 K in the spectrum from Rh(100) surface (grey) is assigned to monolayer methanol-d_4 on the surface.[42,50]

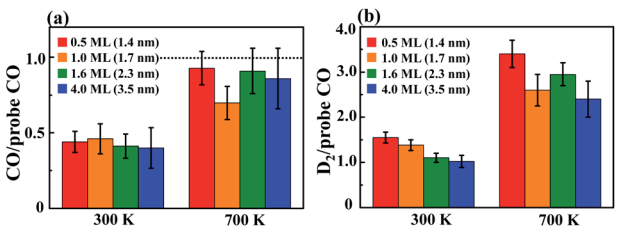

Fig. 4 Ratios of integrated intensities of (a) CO and (b) D_2 TPD spectra from 2.0 L CD_3OD and 2.0 L CO on Rh clusters/Al_2O_3/NiAl(100) as prepared (300 K) and annealed (700 K). The dashed line in (a) indicates the ratios for 0.13 and 0.25 ML Rh (diameter $\leq$ 1.2 nm) at 300 K. The initial Rh coverages 0.5, 1.0, 1.6, 4.0 ML correspond to Rh clusters initially at diameters 1.4, 1.7, 2.3 and 3.5 nm, as indicated in the figure. For 4.0 ML, the lower portions of the clusters became merged.

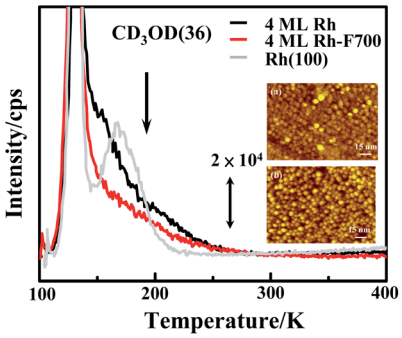

Fig. 5 TPD spectra of CD_3OD (m/z = 36 u) from 2.0 L CD_3OD adsorbed on Rh(100) single crystal and 4.0 ML Rh clusters on Al_2O_3/NiAl(100) as prepared (300 K) and annealed (700 K). The arrow indicates the temperature of the monolayer CD_3OD desorption peak from 2.0 L CD_3OD adsorbed on a thin film of Al_2O_3/NiAl(100). The two insets show the STM images for the 4.0 ML Rh clusters (a) as prepared and (b) annealed.

In contrast, no separate maximum from the desorption of multilayer methanol-d_4 appeared in the spectra from 4.0 ML Rh clusters as prepared (black) and annealed (red), but a shoulder extended from 150 to 270 K. As 4.0 ML Rh clusters both as prepared and annealed covered almost the entire oxide surface (the STM images in Fig. 5), the shoulder is ascribed to monolayer methanol-d_4 desorbing from the Rh clusters. The desorption of CD_3OD from the oxide surface is centered about 190 K, indicated by the arrow in the figure.[44] The intensity of desorption of monolayer methanol-d_4 on the annealed clusters became smaller than that on the clusters as prepared. As the intensity measures the amount of adsorbed monolayer methanol-d_4 that did not react and as the numbers of monolayer methanol-d_4 on the 4.0 ML Rh clusters as prepared and annealed are expected to differ little, the decreased intensity on the annealed clusters confirms the increased reaction probability. Using these desorption data, those of CO_m, which measure the amount of reacting methanol-d_4 (the ionization cross-section for varied species and at varied partial pressure has been considered), and the known rate of dissociation of CO_m,[73] we derived the probability of monolayer methanol-d_4 undergoing dehydrogenation to be 63 $\pm$ 2% on a Rh(100) single crystal, 65 $\pm$ 5% on 4.0 ML Rh clusters as prepared and 86 $\pm$ 3% on annealed 4.0 ML Rh clusters – an increase about 20% in the reaction probability on the annealed 4.0 ML Rh clusters. The dissociation of CO into elementary carbon and oxygen on the present Rh clusters was measured with PES; its rate depended on the cluster size and resembled those earlier studies.[73] It is not straightforward to estimate the reaction probability on the clusters at smaller coverages ($\leq$1.6 ML), as the desorbing CD_3OD might arise partly from the oxide surface (uncovered by the clusters). Nevertheless, the increased reaction probability must be essential in the production of CO_m and D_2 per surface Rh site that increased 2–3 times. More reacting methanol-d_4 on each Rh surface site, possibly resulting from increased density of adsorbed monolayer methanol-d_4 and diffusion of methanol-d_4 molecules from the oxide to the clusters, might contribute to

the effect but cannot account alone for such a great promotion in reactivity.

We have also conducted APXPS measurements to examine whether the promoted reactivity is sustained near ambient pressure. Fig. 6a shows the C 1s spectra from 4.0 ML Rh clusters as prepared on Al_2O_3/NiAl(100) evolving with increased pressure of CD_3OD. The sample temperature was maintained at 400 K, for which methanol-d_4 decomposed to CO_m upon adsorbing on the Rh clusters and a fraction of CO_m desorbed or dissociated to C atoms. The bottom line (Rh – 300 K) in the figure was from the sample with no exposure of CD_3OD. The feature centered about 284.7 eV is assigned to C and that about 286.8 eV to adsorbed CO;[73,74] both were contaminative species. With increasing pressure of CD_3OD, the features of both C and CO grew and shifted positively to 285.0 and 287.1 eV respectively. The growth indicates more CO_m and C produced with increased CD_3OD pressure, and thus active dehydrogenation. The C atoms accumulated notably faster than CO_m; above 10^{-3} torr, the C signals became dominant. It is likely because a fraction of CO_m could desorb whereas all C atoms remained. At 5×10^{-1} torr, all the signals attenuated as the photoelectrons from the sample were scattered by gaseous molecules. Therefore, when the vacuum was back to 5×10^{-7} torr, all the signals were raised (the top line in Fig. 6a). An additional line appeared about 288.9 eV at pressure $\geq 10^{-1}$ torr, which resulted from gaseous CD_3OD.

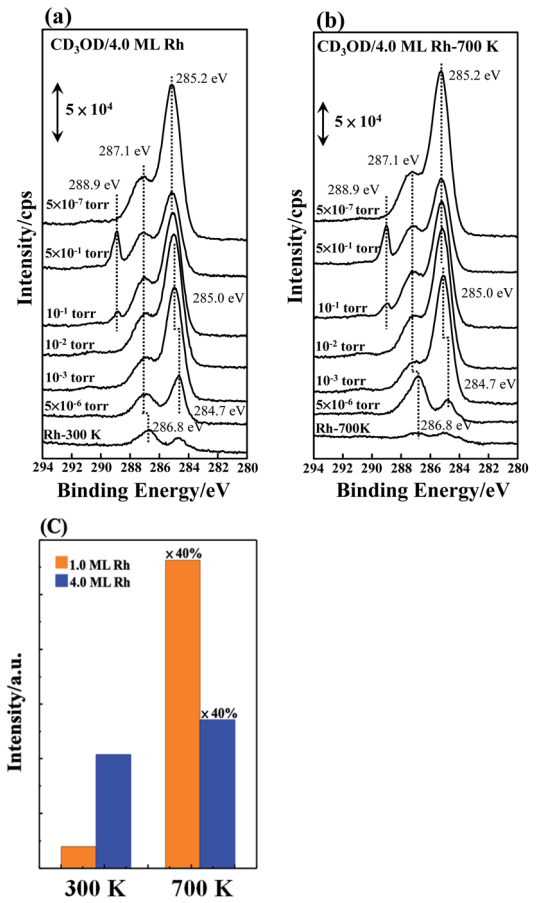

Fig. 6 C 1s photoelectron spectra from 4.0 ML Rh clusters on Al_2O_3/NiAl(100) (a) as prepared (300 K) and (b) annealed (700 K) evolving with increased pressure of CD_3OD from 5×10^{-7} to 5×10^{-1} torr, as indicated. The sample temperature was maintained at 400 K for all the measurements. (c) The ratios of gaseous D_2 signals, measured with a mass spectrometer, at CD_3OD pressure 10^{-1} torr (averages values of 300 s), from 1.0 ML (orange) and 4.0 ML (blue) Rh clusters as-prepared (300 K) and annealed (700 K) to the CO TPD intensities of molecularly CO adsorbed on these Rh clusters as a probe.

Fig. 6b shows the C 1s spectra for annealed (700 K) 4.0 ML Rh clusters on Al_2O_3/NiAl(100) evolving with increased pressure of CD_3OD. The signals for contaminative CO and atomic carbon, the bottom line in the figure, were much less. Like the clusters as prepared, both the CO and C signals were increased and shifted positively with increasing pressure of CD_3OD. The line shapes resembled their counterparts on Rh clusters as prepared but their intensities were in general greater, implying more active dehydrogenation on the annealed Rh clusters. The implication was confirmed by concomitantly monitored gaseous D_2 from the decomposed methanol-d_4 (with a mass spectrometer). As the sample temperature was maintained at 400 K, the produced D_2 was largely desorbed from the surface and readily measured. Fig. 6c compares the ratios of the gaseous D_2 signals (at CD_3OD pressure $= 10^{-1}$ torr) from as-prepared and annealed Rh clusters to the CO TPD intensities of molecularly CO adsorbed on the clusters as a probe. They correspond to the reactivity near ambient pressure and become significantly greater for the annealed clusters (700 K). The promotion in the reactivity was even more prominent under near-ambient-pressure conditions, likely because gaseous CD_3OD was continuously supplied for the reactions. The result agrees with the above TPD ones and further demonstrates that the superior reactivity of annealed Rh clusters is sustained near ambient pressure.

We recorded IRAS spectra in experiments to monitor the dehydrogenation of adsorbed methanol-d_4. The process was activated above 200 K, evidenced by the production of CO_m, but varied little on the annealed clusters. Fig. 7a exemplifies the IRAS spectra of the C–O stretching (ν(CO)) and $\delta_s(CD_3)$ modes of methanol-d_4 on annealed (700 K) 1.6 ML Rh clusters on Al_2O_3/NiAl(100), heated stepwise. The top line, for 2.0 L methanol-d_4 adsorbed on the sample at 110 K, shows two bands: one about 1127 cm^{-1} is assigned to $\delta_s(CD_3)$ mode and the other about 983 cm^{-1} to ν(CO) of methanol-d_4.[75–78] The feature resembles closely those for methanol on Al_2O_3/NiAl(100), Pt, Au–Pt bimetallic clusters.[55,79] With increasing temperature, the ν(CO) and $\delta_s(CD_3)$ modes decreased and vanished about 200 and 225 K, respectively, as adsorbed methanol-d_4 either desorbed or decomposed. Earlier studies shows that methoxy formed from dehydrogenated methanol on Rh single crystals (Rh(100) and Rh(111)) at 140–225 K and that the C–O stretching frequencies (in cm^{-1}) of methanol and methoxy were nearly the same.[40,41] The present ν(CO) frequencies of methanol-d_4 and methoxy-d_3 were also hardly distinguishable. The absorption features of formaldehyde-d_2, which differ drastically from those of methanol-d_4 and methoxy-d_3,[40,80,81] were not observed in our series of experiments.

Fig. 7b shows the corresponding IRAS spectra for the C–O stretching of CO, the O–D and other C–D absorption modes of

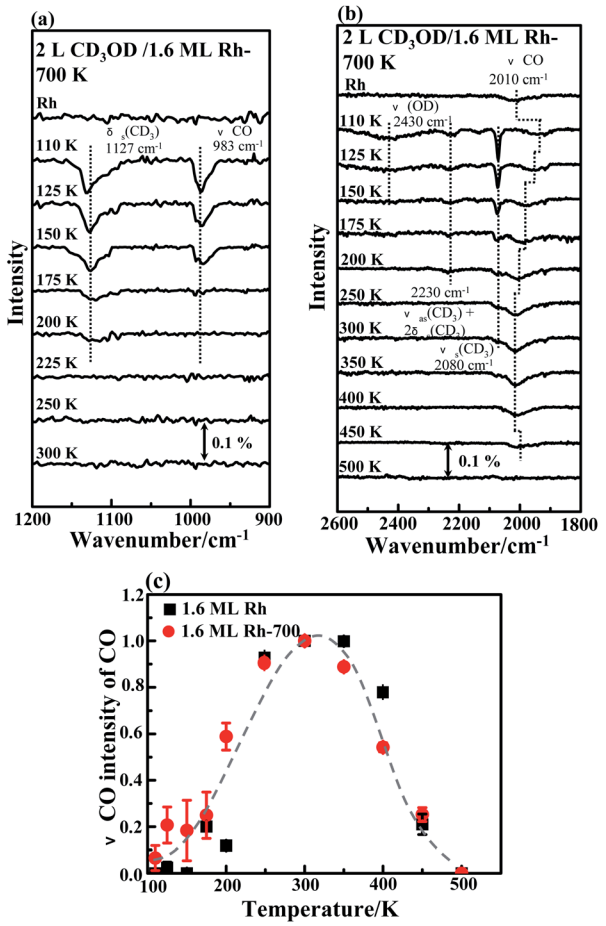

Fig. 7 (a) and (b) IRAS spectra of C–O stretching, C–D and O–D absorption modes for 2.0 L CD_3OD adsorbed on annealed (700 K) 1.6 ML Rh clusters on Al_2O_3/NiAl(100) at 100 K and annealed to selected temperatures; (c) integrated intensities of C–O stretching absorption (ν_{CO}) for CO_m from Rh clusters as prepared (black squares) and annealed (red circles) as a function of temperature. Each spectrum was recorded when the surface was cooled to about 110 K after annealing to the indicated temperature. For (c), the error bars contain the data spread and fitting error. The CO intensities presented were normalized to that obtained at 300 K.

methanol-d_4. The top curve in Fig. 7b, from the annealed Rh clusters before methanol-d_4 adsorption, shows an absorption feature about 2010 cm^{-1}, which is ascribed to contaminative CO on Rh atop sites.[82–84] Upon adsorbing methanol-d_4, the CO features broadened and shifted negatively (the second curve in Fig. 7b), because of the co-adsorbed methanol-d_4.[50,55] The narrow absorption line at 2080 cm^{-1} and the asymmetric absorption centered about 2230 cm^{-1} are assigned to $\nu_s(CD_3)$ and $\nu_{as}(CD_3) + 2\delta_s(CD_3)$ of methanol-d_4, respectively;[75–79] the broad absorption centered near 2430 cm^{-1} is ascribed to the ν(OD) mode of methanol-d_4.[75,77] Upon annealing to 150 K, multilayer methanol-d_4 desorbed, so the intensities in the C–D and O–D regions decreased remarkably. The O–D absorption signals vanished at 150 K because the O–D stretching motion of monolayer methanol-d_4 was nearly parallel to the surface[79] and also because the monolayer methanol-d_4 was partly dehydrogenated to methoxy-d_3. As methanol-d_4 desorbed, the effect of co-adsorbed methanol-d_4 decreased so the CO lines became restored to some extent: both the frequency and intensity increased. On annealing to 175 K, the integrated intensity of the CO line at 175 K exceeded that from contaminative CO (top), implying the onset of dehydrogenation of methanol-d_4 to CO_m. The CO_m signals continued to increase with further increased temperature and attained a maximum about 250–300 K, for which all reacting methanol-d_4 were dehydrogenated to CO_m. The temperature is about 100 K lower than that for adsorbed methanol (350 K),[44] due largely to the isotope effect on the dehydrogenation (scission of C–D and O–D bonds). Elevating the temperature further above 400 K decreased the intensity as CO_m either desorbed (as shown in Fig. 3a and b) or dissociated (observed in previous works).[44,73] The intensity of the $\nu_{as}(CD_3) + 2\delta_s(CD_3)$ mode approached the noise level at 200 K but the $\nu_s(CD_3)$ mode vanished at 250–300 K. The $\nu_s(CD_3)$ and $\nu_{as}(CD_3) + 2\delta_s(CD_3)$ modes of methoxy-d_3 were hardly distinguishable.[40,41,75–78] This decrease again indicates the desorption and dehydrogenation of monolayer methanol-d_4 and methoxy-d_3, consistent with the desorption experiments and the CO IRAS spectra. Similar spectral features were observed for the clusters as prepared (Fig. S3†). Except for the dehydrogenation from methanol-d_4 to methoxy-d_3, which is not clear through our IRAS spectra, the other characteristic reaction processes on Rh clusters both as prepared and annealed differ little.

Fig. 7c plots the variation with temperature of the intensity of the C–O stretching absorption for CO_m (relative to the CO contamination level) on both 1.6 ML Rh clusters as prepared (black squares) and annealed (red circles). Similar variations were shown for the clusters as prepared and annealed: CO_m was produced strongly above 200 K, and the quantity attained a maximum at 250–300 K. The similarity reflects comparable activation energies for the crucial step of CD_3OD dehydrogenation to CO_m on the clusters as prepared and annealed. This crucial step, which was shown previously with DFT simulation to be the dehydrogenation of methoxy to formaldehyde,[44] accounts little for the enhanced reactivity. The altered initial dehydrogenation, the scission of O–D bond, becomes more likely the origin for the promoted reactivity on the annealed Rh clusters.

Discussion

The promoted reactivity on annealed clusters might result from increased methanol-d_4 undergoing dehydrogenation or altered activation energies for dehydrogenation. The former might arise from two mechanisms. First, more methanol-d_4 molecules adsorbed per surface site on annealed clusters, but, as the size and morphology of clusters annealed to 700 K differed only moderately from those of clusters as prepared (Fig. 1), an altered concentration of adsorbed methanol-d_4 must have been limited. The concentration on annealed clusters cannot be 2–3 times that on clusters as prepared, so this mechanism is ineffective. Second, methanol-d_4 adsorbed initially on Al_2O_3/NiAl(100) diffused to Rh clusters to react. As the desorption

temperature of methanol-d_4 on Al_2O_3/NiAl(100), with a maximum about 190 K,[44] was greater than that on Rh, centered about 160 K (Fig. 3), the methanol-d_4 initially on the oxide might diffuse readily to unoccupied Rh sites for the reaction at an elevated temperature. This mechanism might play a role at smaller Rh coverages but is expected to be ineffective at 4.0 ML Rh, for which clusters either as prepared or annealed covered almost the entire oxide surface (the STM image in Fig. 5). The production per Rh site on the annealed 4.0 ML Rh clusters (Fig. 4a) was still enhanced to a value near that of 0.13–0.25 ML Rh as prepared. The increased number of reacting methanol-d_4 must not play an essential role in the promoted reactivity. We argue that the annealing drove changes in surface structures; the newly formed oxide–cluster interfaces provide additional active sites, having smaller activation energies, particularly for the initial dehydrogenation – the O–D bond scission.

The annealing-driven structural alternation was characterized with various techniques. The RHEED measurements exclude evident changes in the atomic stacking inside the clusters after the annealing but not the changes at the oxide–Rh interfaces; significant mass transport, including diffusion of Rh atoms into the substrate and possible migration of alumina materials (Al_xO_y) to the Rh clusters, was indicated and roughened the oxide surface (Fig. 2). The mass transport resulted in new surface sites, reflected on the altered features of D_2 desorption from decomposed methanol-d_4 on annealed clusters – a great proportion of D_2 desorbed at higher temperature (Fig. 3). The new sites are anticipated to be at the oxide–Rh interfaces and likely contain surface Rh and O whose bonding is unsaturated; D atoms are more strongly bonded to such Rh and O. They are active because these low-coordinated Rh and O are more readily to abstract D from adsorbed methanol-d_4. As indicated in earlier study, the competition of the O–D bond scission and desorption of methanol-d_4 determines whether or not the dehydrogenation will proceed.[44] The present system contrasts Pt clusters on Al_2O_3/NiAl(100), for which annealing induced similar mass migration but a decrease in reactivity – the dehydrogenation was hindered to a certain extent.[34] The annealed Pt clusters on Al_2O_3/NiAl(100) were oxidized whereas the annealed Rh clusters exhibited a greater density of electron around Rh atoms. Fig. 8 shows Rh 3d spectra from 1.0 ML Rh clusters grown at 300 K and annealed to 700 K. A shift to greater BE of the Rh 3d with annealing, a feature for oxidized metal clusters,[23,30] was not seen; instead, the Rh 3d shifted to smaller BE (from 308.5 to 308.0 eV for Rh $3d_{5/2}$). Similar shifts were observed for Rh clusters at 0.5 and 3.0 ML (smaller and larger clusters). A negative chemical shift reflects an enhanced screening, due typically to a greater electron density or an electron-richer environment around the atom. An increased size of clusters, a reason frequently seen for such a negative shift of BE, would not account for the shift because the cluster size altered only slightly on annealing to 700 K. The negative shift arises from a charge transfer to the clusters, due to the interaction between Rh and migrating oxides, and/or a decreased coordination of surface Rh. The preceding works show that the low-coordinated surface Rh (with unsaturated bonding) on the clusters, such as edge and corner Rh, have a smaller BE of Rh 3d.[85,86] The corner Rh was indicated earlier to be reactive toward the dehydrogenation of methanol.[44] However, the sole increase of low-coordinated Rh contradicts with the fact that annealing normally improves structural ordering of clusters, indicated also by our RHEED results, and reduces the surface energy, through reducing the number of low-coordinated atoms. Therefore, if the low-coordinated Rh increased, the increased ones should interact or mix with the oxides. The newly formed oxide–Rh interfaces are most likely to provide these reactive low-coordinated Rh. Our results contribute to the knowledge of how metal–support interactions govern the reactivity of oxide-supported metal catalysts. Demonstrated mechanisms of the support effects include oxide (or adsorbates) encapsulation of supported metal nanoclusters,[87–90] small cluster stabilization,[91] charge transfer[92,93] and support participation in catalysis.[87–90,94] The present case constitutes a type of metal–support interactions which promote the reactivity; the metal–support interaction is tuned by annealing to drive the formation of active metal–oxide interfaces.[36]

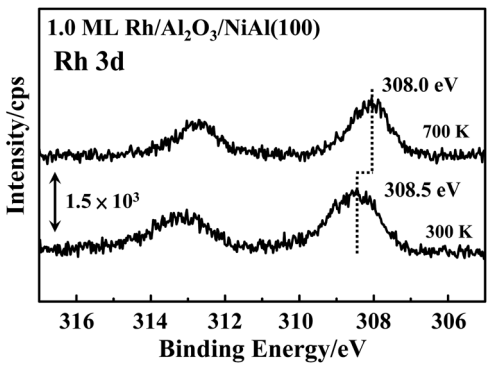

Fig. 8 Rh 3d PES spectra from 1.0 ML Rh clusters prepared at 300 K and annealed to 700 K on Al_2O_3/NiAl(100).

Conclusions

With STM, RHEED, TPD, IRAS, PES and APXPS, we investigated the effect of annealing on the reactivity of supported Rh nanoclusters in the dehydrogenation of methanol-d_4. The Rh clusters were grown with vapor deposition of Rh onto an Al_2O_3/NiAl(100) surface at 300 K; they grew in an fcc phase and (100) orientation, and had a mean diameter 1.0–3.5 nm and height 0.6–0.8 nm. The annealing (700 K) altered little their sizes or lattice parameters, but the support effect on the reactivity *via* a mass transport; the altered Rh–alumina interaction promoted significantly the cluster's reactivity. The quantities of CO_m and D_2 produced from dehydrogenated methanol-d_4 per surface Rh site on the annealed clusters, as a measure of the cluster's reactivity, were enhanced to, at least, 2–3 times those on the as-prepared ones. This enhancement was observed for clusters of diameter >1.2 nm, regardless of cluster sizes, and persisted either under UHV conditions or near ambient pressure. The result demonstrates a type of metal–support interactions which are tunable *via* annealing to promote the reactivity.

Conflicts of interest

There are no conflicts to declare.

Acknowledgements

National Science Council of Taiwan provided support (NSC-100-2112-M-008-010-MY3) for the work. We thank Hsuan Lee and Pei-Yang Cai for their technical support.

References

1 B. Beden, J.-M. Léger and C. Lamy, *Electrocatalytic Oxidation of Oxygenated Aliphatic Organic Compounds at Noble Metal Electrodes*, Plenum Publishers, New York, 1992.
2 G. T. Burstein, C. J. Barnett, A. R. Kucernak and K. R. Williams, *Catal. Today*, 1997, **38**, 425–437.
3 A. Hamnett, *Catal. Today*, 1997, **38**, 445–457.
4 K. R. Williams and G. T. Burstein, *Catal. Today*, 1997, **38**, 401–410.
5 J. R. Rostrup-Nielsen, *Catal. Rev.*, 2004, **46**, 247–270.
6 C. Koenigsmann and S. S. Wong, *Energy Environ. Sci.*, 2011, **4**, 1161–1176.
7 X. Li and A. Faghri, *J. Power Sources*, 2013, **226**, 223–240.
8 N. Kakati, J. Maiti, S. H. Lee, S. H. Jee, B. Viswanathan and Y. S. Yoon, *Chem. Rev.*, 2014, **114**, 12397–12429.
9 Z. Xia, X. Xu, X. Zhang, H. Li, S. Wang and G. Sun, *J. Mater. Chem. A*, 2020, **8**, 1113–1119.
10 L. Jin and Y. Wang, *Phys. Chem. Chem. Phys.*, 2017, **19**, 12992–13001.
11 T. Koitaya, Y. Shiozawa, Y. Yoshikura, K. Mukai, S. Yoshimoto and J. Yoshinobu, *J. Phys. Chem. C*, 2017, **121**, 25402–25410.
12 M. Blatnik, C. Drechsel, N. Tsud, S. Surnev and F. P. Netzer, *J. Phys. Chem. B*, 2018, **122**, 679–687.
13 T.-W. Liao, A. Yadav, P. Ferrari, Y. Niu, X.-K. Wei, J. Vernieres, K.-J. Hu, M. Heggen, R. E. Dunin-Borkowski, R. E. Palmer, K. Laasonen, D. Grandjean, E. Janssens and P. Lievens, *Chem. Mater.*, 2019, **31**, 10040–10048.
14 C. T. Campbell, *Surf. Sci. Rep.*, 1997, **27**, 1–111.
15 C. R. Henry, *Surf. Sci. Rep.*, 1998, **31**, 231–233, 235–325.
16 T. P. St. Clair, X. Lai, M. Valden and D. W. Goodman, *Prog. Surf. Sci.*, 1998, **59**, 25–52.
17 M. Bäumer and H.-J. Freund, *Prog. Surf. Sci.*, 1999, **61**, 127–198.
18 A. K. Santra and D. W. Goodman, *J. Phys.: Condens. Matter*, 2002, **14**, R31–R62.
19 S. K. Shaikhutdinov, R. Meyer, M. Naschitzki, M. Bäumer and H.-J. Freund, *Catal. Lett.*, 2003, **86**, 211–219.
20 C. Lemire, R. Meyer, S. K. Shaikhutdinov and H.-J. Freund, *Surf. Sci.*, 2004, **552**, 27–34.
21 R. Meyer, D. Lahav, T. Schalow, M. Laurin, B. Brandt, S. Schauermann, S. Guimond, T. Klüner, H. Kuhlenbeck, J. Libuda, S. Shaikhutdinov and H. J. Freund, *Surf. Sci.*, 2005, **586**, 174–182.
22 M. F. Luo, C. I. Chiang, H. W. Shiu, S. D. Sartale, T. Y. Wang, P. L. Chen and C. C. Kuo, *J. Chem. Phys.*, 2006, **124**, 164709.
23 M.-F. Luo, M.-H. Tien, C.-C. Wang, W.-R. Lin, J.-Y. Ho, B.-W. Chang, C.-T. Wang, Y.-C. Lin and Y.-J. Hsu, *J. Phys. Chem. C*, 2009, **113**, 12419–12426.
24 M.-F. Luo, C.-C. Wang, C.-S. Chao, C.-Y. Ho, C.-T. Wang, W.-R. Lin, Y.-C. Lin, Y.-L. Lai and Y.-J. Hsu, *Phys. Chem. Chem. Phys.*, 2011, **13**, 1531–1541.
25 H. Khosravian, Y. Lei, A. Uhl, M. Trenary and R. J. Meyer, *Chem. Phys. Lett.*, 2013, **555**, 7–11.
26 Y. Lei, A. Uhl, C. Becker, K. Wandelt, B. C. Gates, R. Meyer and M. Trenary, *Phys. Chem. Chem. Phys.*, 2010, **12**, 1264–1270.
27 Y. Lykhach, J. Pešička and V. Nehasil, *Vacuum*, 2001, **63**, 283–289.
28 S. Penner and M. Armbrüster, *ChemCatChem*, 2015, **7**, 374–392.
29 T. W. van Deelen, C. Hernández Mejía and K. P. de Jong, *Nat. Catal.*, 2019, **2**, 955–970.
30 E. Ozensoy, C. H. F. Peden and J. Szanyi, *J. Phys. Chem. B*, 2006, **110**, 17001–17008.
31 J. R. Croy, S. Mostafa, L. Hickman, H. Heinrich and B. R. Cuenya, *Appl. Catal., A*, 2008, **350**, 207–216.
32 G. N. Vayssilov, Y. Lykhach, A. Migani, T. Staudt, G. P. Petrova, N. Tsud, T. Skála, A. Bruix, F. Illas, K. C. Prince, V. Matolín, K. M. Neyman and J. Libuda, *Nat. Mater.*, 2011, **10**, 310–315.
33 M. Happel, J. Mysliveček, V. Johánek, F. Dvořák, O. Stetsovych, Y. Lykhach, V. Matolín and J. Libuda, *J. Catal.*, 2012, **289**, 118–126.
34 C. S. Chao, Y. D. Li, T. W. Liao, T. C. Hung and M. F. Luo, *Appl. Surf. Sci.*, 2014, **311**, 763–769.
35 H. Tang, Y. Su, B. Zhang, A. F. Lee, M. A. Isaacs, K. Wilson, L. Li, Y. Ren, J. Huang, M. Haruta, B. Qiao, X. Liu, C. Jin, D. Su, J. Wang and T. Zhang, *Sci. Adv.*, 2017, **3**, e1700231.
36 I. Ro, J. Resasco and P. Christopher, *ACS Catal.*, 2018, **8**, 7368–7387.
37 X. Du, Y. Huang, X. Pan, B. Han, Y. Su, Q. Jiang, M. Li, H. Tang, G. Li and B. Qiao, *Nat. Commun.*, 2020, **11**, 5811.
38 H. O. Otor, J. B. Steiner, C. García-Sancho and A. C. Alba-Rubio, *ACS Catal.*, 2020, **10**, 7630–7656.
39 F. Solymosi, A. Berkó and T. I. Tarnóczi, *Surf. Sci.*, 1984, **141**, 533–548.
40 C. Houtman and M. A. Barteau, *Langmuir*, 1990, **6**, 1558–1566.
41 J. E. Parmeter, J. Xudong and D. W. Goodman, *Surf. Sci.*, 1990, **240**, 85–100.
42 R. Jiang, W. Guo, M. Li, H. Zhu, L. Zhao, X. Lu and H. Shan, *J. Mol. Catal. A: Chem.*, 2011, **344**, 99–110.
43 J. Zhou and D. R. Mullins, *J. Phys. Chem. B*, 2006, **110**, 15994–16002.
44 T.-C. Hung, T.-W. Liao, Z.-H. Liao, P.-W. Hsu, P.-Y. Cai, H. Lee, Y.-L. Lai, Y.-J. Hsu, H.-Y. Chen, J.-H. Wang and M.-F. Luo, *ACS Catal.*, 2015, **5**, 4276–4287.
45 P. Gassmann, R. Franchy and H. Ibach, *Surf. Sci.*, 1994, **319**, 95–109.
46 R.-P. Blum, D. Ahlbehrendt and H. Niehus, *Surf. Sci.*, 1998, **396**, 176–188.

47 S. Schauermann, J. Hoffmann, V. Johánek, J. Hartmann, J. Libuda and H.-J. Freund, *Catal. Lett.*, 2002, **84**, 209–217.
48 N. Frémy, V. Maurice and P. Marcus, *J. Am. Ceram. Soc.*, 2003, **86**, 669–675.
49 M. C. Zei, C.-S. Lin, W.-H. Wen, C.-I. Chiang and M.-F. Luo, *Surf. Sci.*, 2006, **600**, 1942–1951.
50 G.-R. Hu, C.-S. Chao, H.-W. Shiu, C.-T. Wang, W.-R. Lin, Y.-J. Hsu and M.-F. Luo, *Phys. Chem. Chem. Phys.*, 2011, **13**, 3281–3290.
51 H. Qin, P. Sutter and G. Zhou, *J. Am. Ceram. Soc.*, 2014, **97**, 2762–2769.
52 H. Qin, X. Chen, L. Li, P. W. Sutter and G. Zhou, *Proc. Natl. Acad. Sci. U. S. A.*, 2015, **112**, E103–E109.
53 S. Schauermann, J. Hoffmann, V. Johánek, J. Hartmann and J. Libuda, *Phys. Chem. Chem. Phys.*, 2002, **4**, 3909–3918.
54 M. Bäumer, J. Libuda, K. M. Neyman, N. Rösch, G. Rupprechter and H. J. Freund, *Phys. Chem. Chem. Phys.*, 2007, **9**, 3541–3558.
55 C.-S. Chao, Y.-D. Li, B.-W. Hsu, W.-R. Lin, H.-C. Hsu, T.-C. Hung, C.-C. Wang and M.-F. Luo, *J. Phys. Chem. C*, 2013, **117**, 5667–5677.
56 A. Cho, *Science*, 2003, **299**, 1684–1685.
57 M.-F. Luo, C.-I. Chiang, H.-W. Shiu, S. D. Sartale and C.-C. Kuo, *Nanotechnol*, 2006, **17**, 360–366.
58 M.-F. Luo, W.-H. Wen, C.-S. Lin, C.-I. Chiang, S. D. Sartale and M. C. Zei, *Surf. Sci.*, 2007, **601**, 2139–2146.
59 I. Hong, T. H. Lee, G. Yin, D. Wei, J. Juang, T. E. Dann, R. Klauser, T. Chuang, C. Chen and K. Tsang, *Nucl. Instrum. Methods Phys. Res., Sect. A*, 2001, **467–468**, 905–908.
60 C.-H. Wang, S.-T. Chang, S.-Y. Chen and Y.-W. Yang, *AIP Conf. Proc.*, 2019, **2054**, 040012.
61 V. Maurice, N. Frémy and P. Marcus, *Surf. Sci.*, 2005, **581**, 88–104.
62 J. F. Moulder, W. F. Stickle, P. E. Sobol and K. D. Bomben, *Handbook of X-ray Photoelectron Spectroscopy*, Physical Electronics Inc. USA, 1995.
63 M. F. Luo, H. W. Shiu, M. H. Ten, S. D. Sartale, C. I. Chiang, Y. C. Lin and Y. J. Hsu, *Surf. Sci.*, 2008, **602**, 241–248.
64 Z.-H. Liao, P.-W. Hsu, T.-C. Hung, G. Liao Jr, Z.-Y. Chern, Y.-L. Lai, L.-C. Yu, Y.-J. Hsu, J.-H. Wang, P. Chen and M.-F. Luo, *Catalysts*, 2019, **9**, 971.
65 M.-F. Luo, C.-C. Wang, G.-R. Hu, W.-R. Lin, J.-Y. Ho, Y.-C. Lin and Y.-J. Hsu, *J. Phys. Chem. C*, 2009, **113**, 21054–21062.
66 J. Stubenrauch and J. M. Vohs, *Catal. Lett.*, 1997, **47**, 21–25.
67 E. S. Putna, R. J. Gorte, J. M. Vohs and G. W. Graham, *J. Catal.*, 1998, **178**, 598–603.
68 T.-C. Hung, T.-W. Liao, Z.-H. Liao, P.-W. Hsu, P.-Y. Cai, W.-H. Lu, J.-H. Wang and M.-F. Luo, *RSC Adv.*, 2016, **6**, 3830–3839.
69 The concentration of CO (number of CO per surface site) on the Rh clusters varies with the cluster size (ref. 68).
70 B. A. Sexton, *Surf. Sci.*, 1981, **102**, 271–276.
71 J. Wang and R. I. Masel, *J. Am. Chem. Soc.*, 1991, **113**, 5850–5856.
72 N. Kizhakevariam and E. M. Stuve, *Surf. Sci.*, 1993, **286**, 246–260.
73 S. Andersson, M. Frank, A. Sandell, A. Giertz, B. Brena, P. A. Brühwiler, N. Mårtensson, J. Libuda, M. Baümer and H.-J. Freund, *J. Chem. Phys.*, 1998, **108**, 2967.
74 M. Frank, S. Andersson, J. Libuda, S. Stempel, A. Sandell, B. Brena, A. Giertz, P. A. Brühwiler, M. Bäumer, N. Mårtensson and H. J. Freund, *Chem. Phys. Lett.*, 1997, **279**, 92–99.
75 J. S. Huberty and R. J. Madix, *Surf. Sci.*, 1996, **360**, 144–156.
76 W. S. Sim, P. Gardner and D. A. King, *J. Phys. Chem.*, 1995, **99**, 16002–16010.
77 R. B. Barros, A. R. Garcia and L. M. Ilharco, *J. Phys. Chem. B*, 2001, **105**, 11186–11193.
78 S. J. Pratt, D. K. Escott and D. A. King, *J. Chem. Phys.*, 2003, **119**, 10867.
79 Y.-D. Li, T.-W. Liao, C. X. Wang, C.-S. Chao, T.-C. Hung, C. Y. Ho, M.-F. Luo, Y.-L. Lai and Y.-J. Hsu, *RSC Adv.*, 2014, **4**, 31602.
80 M. A. Henderson, G. E. Mitchell and J. M. White, *Surf. Sci.*, 1987, **188**, 206–218.
81 C. Houtman and M. A. Barteau, *Surf. Sci.*, 1991, **248**, 57–76.
82 M. Frank, R. Kühnemuth, M. Bäumer and H. J. Freund, *Surf. Sci.*, 1999, **427–428**, 288–293.
83 G. Krenn, I. Bako and R. Schennach, *J. Chem. Phys.*, 2006, **124**, 144703.
84 H. P. Koch, P. Singnurkar, R. Schennach, A. Stroppa and F. Mittendorfer, *J. Phys. Chem. C*, 2008, **112**, 806–812.
85 F. Strisland, A. Ramstad, T. Ramsvik and A. Borg, *Surf. Sci.*, 1998, **415**, L1020–L1026.
86 A. Cavallin, M. Pozzo, C. Africh, A. Baraldi, E. Vesselli, C. Dri, G. Comelli, R. Larciprete, P. Lacovig, S. Lizzit and D. Alfè, *ACS Nano*, 2012, **6**, 3034.
87 S. J. Tauster, S. C. Fung and R. L. Garten, *J. Am. Chem. Soc.*, 1978, **100**, 170–175.
88 A. K. Datye, D. S. Kalakkad, M. H. Yao and D. J. Smith, *J. Catal.*, 1995, **155**, 148–153.
89 O. Dulub, W. Hebenstreit and U. Diebold, *Phys. Rev. Lett.*, 2000, **84**, 3646–3649.
90 J. C. Matsubu, S. Zhang, L. DeRita, N. S. Marinkovic, J. G. Chen, G. W. Graham, X. Pan and P. Christopher, *Nat. Chem.*, 2017, **9**, 120–127.
91 J. A. Farmer and C. T. Campbell, *Science*, 2010, **329**, 933–936.
92 A. Bruix, J. A. Rodriguez, P. J. Ramírez, S. D. Senanayake, J. Evans, J. B. Park, D. Stacchiola, P. Liu, J. Hrbek and F. Illas, *J. Am. Chem. Soc.*, 2012, **134**, 8968–8974.
93 C. T. Campbell, *Nat. Chem.*, 2012, **4**, 597–598.
94 J. Graciani, K. Mudiyanselage, F. Xu, A. E. Baber, J. Evans, S. D. Senanayake, D. J. Stacchiola, P. Liu, J. Hrbek, J. F. Sanz and J. A. Rodriguez, *Science*, 2014, **345**, 546–550.